



Embryonic Mesenchymal Multipotent Cell Differentiation on Electrospun Biodegradable Poly(ester amide) Scaffolds for Model Vascular Tissue Fabrication

SARAH KIROS,¹ SHIGANG LIN,² MALCOLM XING,³ and KIBRET MEQUANINT ^{1,2}

¹School of Biomedical Engineering, University of Western Ontario, London, ON N6A 5B9, Canada; ²Department of Chemical & Biochemical Engineering, University of Western Ontario, London, ON N6A 5B9, Canada; and ³Department of Mechanical Engineering, University of Manitoba, 66 Chancellors Circle, Winnipeg R3T 2N2, Canada

(Received 3 February 2019; accepted 22 April 2019; published online 6 May 2019)

Associate Editor Jane Grande-Allen oversaw the review of this article.

Abstract—Vascular differentiation of stem cells and matrix component production on electrospun tubular scaffolds is desirable to engineer blood vessels. The mouse embryonic multipotent mesenchymal progenitor cell line (10T1/2) provides an excellent tool for tissue engineering since it shares similar differentiation characteristics with mesenchymal stem cells. Although 10T1/2 cells have been widely studied in the context of skeletal tissue engineering, their differentiation to smooth muscle lineage is less known. In this study, we fabricated tubular electrospun poly(ester amide) (PEA) fibers from L-phenylalanine-derived biodegradable biomaterials and investigated cell-scaffold interactions as well as their differentiation into vascular smooth muscle cell and subsequent elastin expression. PEA scaffolds fabricated under different collector speeds did not have an impact on the fiber directionality/orientation. 10T1/2 cytocompatibility and proliferation studies showed that PEA fibres were not cytotoxic and were able to support proliferation for 14 days. Furthermore, cells were observed infiltrating the fibrous scaffolds despite the small pore sizes (~ 5 μm). Vascular differentiation studies of 10T1/2 cells using qPCR, Western blot, and immunostaining showed a TGF β 1-induced upregulation of vascular smooth muscle cell (VSMC)-specific markers smooth muscle alpha-actin (SM- α -actin) and smooth muscle myosin heavy chain (SM-MHC). Differentiated 10T1/2 cells produced both elastin and fibrillin-1 suggesting the potential of fibrous PEA scaffolds to fabricate model vascular tissues.

Keywords—Poly(ester amide)s, 10T1/2 cell differentiation, Tubular electrospinning, Vascular smooth muscle cells, Elastin, Fibrillin-1.

INTRODUCTION

Despite considerable advances made in vascular tissue engineering strategies, challenges remain. Such challenges include cell sources and scaffolding materials.³³ With regards to cells, induced pluripotent stem cells (iPSC), adult stem cells, and progenitor cells are promising alternatives to primary vascular smooth muscle cells (VSMC) and endothelial cells due to their increased proliferative capacity, potential to differentiate into vascular lineages with the addition of soluble growth factors^{7,20,33} and their ability to circumvent the ethical concerns surrounding the use of embryonic stem cells. However, *in vitro* stem cell differentiation into a target lineage is not always successful. Although differentiation markers for the target lineage may be positive, this does not guarantee a lack of other diversity during the process.

Since one of the aims of tissue engineering is to develop *in vitro* model tissues for fundamental studies of vascular disease and biology, well-characterized progenitor cells could be advantageous. Mesenchymal multipotent C3H10T1/2 cells, commonly referred to as 10T1/2 cells are a clonal cell line derived from mouse embryos, and may serve as a good *in vitro* model for vascular differentiation studies due to their undemanding culture conditions and their ability to differentiate to VSMC in 2D culture using only one growth factor (e.g. TGF- β 1).⁴⁶ In fact, by seeding a mesenchymal multipotent progenitor cell line (10T1/2 cells) on non-degradable polyurethane scaffolds, we previously fabricated vascular tissues having substantial elastin.²¹ However, since the scaffold was non-

Address correspondence to Kibret Mequanint, Department of Chemical & Biochemical Engineering, University of Western Ontario, London, ON N6A 5B9, Canada. Electronic mail: kmequani@uwo.ca

degradable, the polyurethane permanently remained in the final tissue which is not desirable. Furthermore, because our previous study²¹ was on biostable scaffolds, it is unknown if the biodegradation by-products of a scaffold could be detrimental to 10T1/2 cell differentiation into smooth muscle cells and subsequent elastin deposition. Therefore, investigating biodegradable scaffolds is the next step towards utilizing these cells to engineer model vascular tissues.

In addition to choosing cells, the design of biodegradable biomaterials and scaffolds is an important consideration for tissue engineering and regenerative medicine applications. Depending on the intended applications, biodegradable scaffolds may be fabricated from soft or rigid materials with variable degradation rate and time. For instance, porcine carotid arteries have been decellularized and used as a scaffold to fabricate small-diameter vascular tissues potentially accelerating the maturation process due to the structural and functional properties of extracellular matrix (ECM) proteins.^{9,10} Although naturally-occurring scaffolds such as decellularized ECM, fibrin, and collagen gels have been used to fabricate vascular tissues,³⁹ synthetic scaffolds are often versatile since their properties can easily be modified to suit specific needs. While degradable polyesters from α -hydroxy acids, lactic acid, and glycolic acid are most commonly used, biodegradable poly(ester amide)s (PEAs)—bearing both ester and amide repeat units—have emerged to be attractive.^{4,18,19} Since ester and amide repeat units along the PEA chain can be introduced using a variety of starting materials, the name PEA does not represent one specific structure or composition. Instead, it is a generic name given to a library of polymers with ester and amide repeat units regardless of the diverse starting materials used to prepare them.^{8,44} Because of this, both biodegradable and biostable PEAs can be designed for different applications.^{14,44}

In the context of tissue engineering and regenerative medicine, PEAs derived from biodegradable precursors with the potential to promote cell attachment, spreading, and differentiation are most favoured. In view of this, we have previously reported the synthesis and characterization of a library of PEAs derived from naturally-occurring amino acids.^{4,18} The balance between the acidic and basic degradation products provided a buffering effect thus limiting the downward pH drift³⁴ which otherwise is known to negatively impact cell behaviour.³⁶ Despite their versatility as a film, fabrication of fibrous scaffolds required blending them with polycaprolactone (PCL).³⁴ Further synthesis optimization allowed us to prepare PEAs that are electrospinnable.¹⁹ These PEAs have been investigated for VSMC interactions^{18,19} and vascular growth factor

delivery^{28,29} applications; however, these studies have used differentiated primary cells,³⁴ and the ability of these materials to support vascular differentiation of progenitor cells has yet to be explored. Furthermore, PEAs have not been electrospun into tubular scaffolds.

In view of the above, the objectives of the present study were three-fold: (i) to fabricate tubular PEA scaffolds by electrospinning and evaluate fiber morphology, diameter, and directionality, (ii) to investigate mesenchymal multipotent 10T1/2 progenitor cells interactions and differentiation towards vascular lineage and (iii) to evaluate the extent to which these cells produce elastin on PEA scaffolds.

MATERIALS AND METHODS

PEA Biomaterial

The PEA biomaterial used in this study was prepared by interfacial polymerization as previously reported.¹⁸ Briefly, L-phenylalanine (60.8 mM, 2.2 equivalents), *p*-toluenesulfonic acid monohydrate (66.3 mM, 2.4 equivalent), and 1,4-butanediol (27.6 mM, 1 equivalent) in toluene (100 mL) were reacted at 140 °C for 48 h and purified by crystallization to get the *di-p*-toluenesulfonic acid salt monomer. Sebacyl chloride (5 mM, 1 equivalent) was then dissolved in glass distilled anhydrous dichloromethane (15 mL) and the solution was added dropwise to an aqueous solution (15 mL) containing *di-p*-toluenesulfonic acid salt monomer (5.0 mM, 1 equivalent) and sodium carbonate (10 mM, 2 equivalents), and allowed to react for 16 h. Once the reaction was complete, a rotary evaporator was used in order to remove residual dichloromethane. The polymer was then washed with deionized water prior to purification *via* Soxhlet extraction with ethyl acetate for 48 h, followed by drying under vacuum for 72 h¹⁸ ($M_n = 55$ kDa, PDI 2.0).

Electrospinning of PEA Tubular Scaffold

The electrospinning setup consisted of a high voltage DC Power Supply (ES30P, Gamma high voltage, USA), a glass syringe (Becton, Dickinson and Co., 0.5 mL, NJ, USA) with a blunt-tip stainless steel needle controlled by a syringe pump (KD101, KD scientific, USA), and a stainless steel rotating mandrel (4 mm diameter). Prior to electrospinning, the rotating mandrel was coated with Span80 (Sigma-Aldrich, Milwaukee, WI) to facilitate the removal of the fibers and preserve its tubular structure. Formulation parameters were kept constant at 6% w/w in 9:1 w/w chloroform: dimethylsulfoxide (DMSO), in order to obtain bead-free fibers with uniform fiber diameter

distribution. The rotational speeds were set to 150, 1000, and 2000 rpm.

Scanning Electron Microscopy (SEM)

The morphology of the PEA fibers was visualized using SEM, (S-2600 N, Hitachi, Japan); tubular scaffolds were cut into square mats to facilitate the imaging of the fibrous structure. Samples were mounted on carbon-taped aluminum stubs and sputtered with gold/palladium (K550X, sputter coater, Emitech Ltd., UK) at 15 mA for 3 to 5 min prior to analysis. Samples were scanned at a working distance of 9 mm and an accelerating voltage of 5 kV. Fiber diameter distributions were assessed using ImageJ software (NIH, Bethesda, MD), where sample sizes of 100 fibers from three separate images were measured for each fiber diameter distribution and ImageJ directionality plug-in was utilized to determine the preferred fiber orientation.³¹

Metabolic Activity and Cell Proliferation Assays

Mouse embryo multipotent mesenchymal progenitor cells (C3H/10T1/2 cells; ATCC; Manassas, VA) were maintained in high glucose DMEM with 5% fetal bovine serum, incubated at 37 °C and 5% CO₂, and passaged just before reaching confluence. Circular samples (4 mm in diameter) of electrospun mats were punched and affixed to a 96-well cell culture plate (BD Falcon, Franklin Lakes, NJ) using silicone grease, and disinfected by immersion in 70% ethanol (100 μL) for 30 min, before conditioning overnight in Hank's balanced salt solution (HBSS, 100 μL; Invitrogen Canada, Burlington, ON). For cytotoxicity, 3-(4,5-dimethylthiazol-2-yl)-2,5-diphenyltetrazolium bromide (MTT) assay was performed following the manufacturer's protocol (Vybrant[®], Invitrogen, Burlington, ON, Canada). First, cells were seeded onto electrospun PEA at 1000 cells/scaffold which were then cultured in DMEM supplemented with 1% penicillin/streptomycin (P/S) solution and 5% FBS for 3, 7 and 14 days, respectively. The medium was refreshed (100 μL) every 3 to 4 days. At the pre-determined time points, 12 mM MTT solution was added to each well and then incubated at 37 °C for 4 h. Afterwards, 100 μL 10% (w/v) SDS was added to solubilize the formazan, and further incubated at 37 °C for 18 h. The absorbance of the coloured product was recorded at 562 nm by a microplate reader in a 96-well plate. Negative control experiments were conducted by adding MTT to the culture medium only and were subtracted from the samples to obtain the final reading.

DNA quantification was assessed using the CyQUANT cell proliferation assay (ThermoFisher Scientific, Burlington, ON). Briefly, the cell-seeded PEA scaffolds were removed from the incubator at 3, 7 and 14 days, washed three times with 1 × PBS, placed in microcentrifuge tubes, and frozen at - 80 °C until assayed. The cells were thawed at room temperature, and 100 μL of CyQUANT GR dye/cell lysis buffer was added to each microcentrifuge tube to release the DNA from the scaffolds. The supernatant was collected and the fluorescence intensity was measured on an M1000 Infinite Pro microplate (Tecan Inc. Morrisville, NC) at an excitation wavelength of 480 nm and an emission wavelength of 520 nm.

Immunofluorescence Staining and Laser Scanning Confocal Microscopy

10T1/2 cell attachment, spreading and infiltration were assessed for electrospun PEA scaffolds using confocal microscopy. The culture time for immunofluorescence studies was for 14 days on PEA fibrous tubes. Cells were washed with ice-cold PBS immediately prior to fixing at room temperature for 15 min in 4% formaldehyde solution (1 mL; EMD Chemicals) in divalent cation-free PBS. Following three washes in PBS, 10T1/2 cells were permeabilized with 0.1% Triton X-100 (0.5 mL; VWR International, Mississauga, ON) in PBS for 5 min and again washed three times with PBS. The cells were incubated with 1% BSA in PBS (0.5 mL; Sigma-Aldrich, Oakville, ON) for 30 min at room temperature prior to their incubation with primary antibodies. For immunofluorescence staining, primary mouse anti-SM- α -actin (1:50; Santa Cruz.), rabbit anti-SM-MHC (1:50; BT Inc.), rabbit anti-elastin (1:50; EPC) and mouse anti-fibrillin-1 (1:50; EMD Millipore) were used. Primary antibody binding was detected using Alexa Fluor[®] 555 goat anti-rabbit IgG or Alexa Fluor[®] 488 goat anti-mouse IgG as secondary antibodies (1:300; Life Technologies, Burlington, ON) addition with Alexa Fluor[®] 568- or Alexa Fluor[®] 488 phalloidin (1:100 dilution; Invitrogen Canada, Burlington, ON) for detecting F-actin in the dark for 1 h at room temperature followed by another three washes with PBS. The cells were then counterstained with 4'-6-diamidino-2-phenylindole dihydrochloride (DAPI, 300 nM in PBS, 0.5 mL; Invitrogen Canada, Burlington, ON) for 5 min to label the nuclei and again washed three times with PBS. Coverslips were mounted on microscope slides with PermaFluor[™] Mounting Medium (Thermo Scientific[™], Canada) and sealed with clear nail enamel. Images were taken with a Zeiss LSM 510

confocal microscope (Zeiss, Canada) equipped with an argon/neon as well as a UV laser.

qPCR and Western Blot Analyses

10T1/2 cells were seeded at a density of $2.5\text{--}5.0 \times 10^5$ cells per scaffold on 12-well plates (circular specimens 1.9 cm in diameter). RNA was extracted using Trizol reagent (Life Technologies) following the manufacturer's instructions. Complementary DNA (cDNA) was synthesized using $1\ \mu\text{g}$ of total RNA primed with random primers as described in PromegaTM Random Hexamers protocol (Fisher Scientific, Canada). qPCR was conducted in $10\ \mu\text{L}$ reaction volumes, using a CFX96TM Real-Time System (C1000 Touch Thermal Cycler; Bio-Rad, Canada) and gene expression of glyceraldehyde-3-phosphate dehydrogenase (GAPDH), SM- α -actin, and SM-MHC were determined with iQTM SYBR[®] Green Supermix (Bio-Rad) according to the recommended protocol of the manufacturer. The sequences of primers were designed using Primer3Web. SM- α -actin forward primer 5'-GGG CTA TAT AAC CCT TCA GCG-3', reverse primer: 3'-GCT GTC TTC CTC TTC ACA CAT-5'. GAPDH forward primer 5'-GGT GGT CTC CTC TGA CTT CAA CA-3' reverse primer 3'-GTT GCT GTA GCC AAA TTC GTT GT-5'. SM-MHC forward primer 5'-CTG GTT ACA TTG TAG GTG CCA-3', reverse primer 3'-GCG AGC AGG TAG TAG AA GAT G-5'. The results were analyzed with the comparative threshold cycle method and normalized with GAPDH as an endogenous reference.

Western blotting was performed to evaluate the expression levels of VSMC phenotypic marker proteins. At day 7, cells were washed three times with ice-cold PBS and whole cell lysates were obtained by harvesting cells in $100\ \mu\text{L}$ of sodium dodecyl sulfate electrophoresis sample buffer containing 5% (v/v) β -mercaptoethanol. Lysates were sonicated, microcentrifuged, and the protein concentrations were determined by 660 nm Protein Assay (Thermo Scientific, Ottawa, Canada). Protein samples ($30\ \mu\text{g}$) were separated by 10% sodium dodecyl sulfate/polyacrylamide gel electrophoresis (SDS-PAGE) and transferred at 90 V for 1 h at room temperature to a nitrocellulose membrane in a Tris-glycine buffer. Transfer efficiency was assessed by Ponceau red stain. Nitrocellulose membranes were blocked with 5% nonfat dry milk in PBS and incubated overnight at $4\ ^\circ\text{C}$ with primary antibodies (anti SM- α -actin 1:1000; anti-GAPDH (1:5000, Millipore); anti-SM-MHC IgG (1:500; Biomedical Technologies Inc). The blots were probed with HRP-conjugated secondary antibodies followed by the ECL detection (ThermoFisher Scientific) according to manufacturer's specifications with a

Molecular Imager ChemiDocTM XRS + system (Bio-Rad Laboratories (Canada) Ltd., Mississauga, ON).

Statistical Analysis

Where applicable, results were presented as mean \pm SD from at least three independent experiments and were statistically analyzed either by unpaired Student's *t* test or by two-way ANOVA. For the MTT assay, the two-way ANOVA was followed by Tukey's *post hoc* test to compare the differences between groups, using GraphPad Prism 6. Significant differences were assumed for $p < 0.05$.

RESULTS AND DISCUSSION

PEA Electrospinnability, Fibre Morphology, and Orientation

PEAs of the type used in this study are emerging biomaterials that have not been well-studied in terms of electrospinning into tubular structures. PEAs aside, it is generally challenging to fabricate tubular tissue engineering scaffolds from other biomaterials which are evident from relatively lower numbers of studies compared with other electrospun scaffold shapes.^{5,32,38,41} Before fabricating the tubular fibrous PEA scaffolds, we established the conditions (PEA concentration and solvent ratio along with applied voltage, flow rate, and distance to collector) to produce beads-free fibers. In these screening experiments (data not shown), we have optimized the PEA concentration between 5 and 7% w/w at a flow rate of 0.1 mL/h. Below 5% PEA concentration, the solution was electrospayed with little fibers formed and above 7%, the solution rapidly dried at the needle tip, due to the quick evaporation of chloroform that increased the viscosity. Increasing the DMSO solvent content above 10% led to fiber fusion at the collector due to its slow evaporation during the jet formation. Having established the spinning parameters, we fabricated tubular fibrous scaffolds having 5 mm diameter (Fig. 1a). The wall thickness produced was $\sim 130\text{--}150\ \mu\text{m}$ (0.13–0.15 mm) as determined from SEM images. Since the rotational speed of the collector is believed to have some effect on fiber morphology and directionality, we studied three rotational speeds (150, 1000, and 2000 rpm). All rotational speeds yielded fibers that were free from beads (Figs. 1b–1d). The pore sizes of the fibrous scaffolds were up to $5\ \mu\text{m}$ (Fig. 1e) and were similar for all three different collector speeds. The fiber diameters were not affected by the collector speed as the average diameter was between 250 nm and 300 nm as shown by the histograms of the corresponding collector rpm (Fig. 1f).

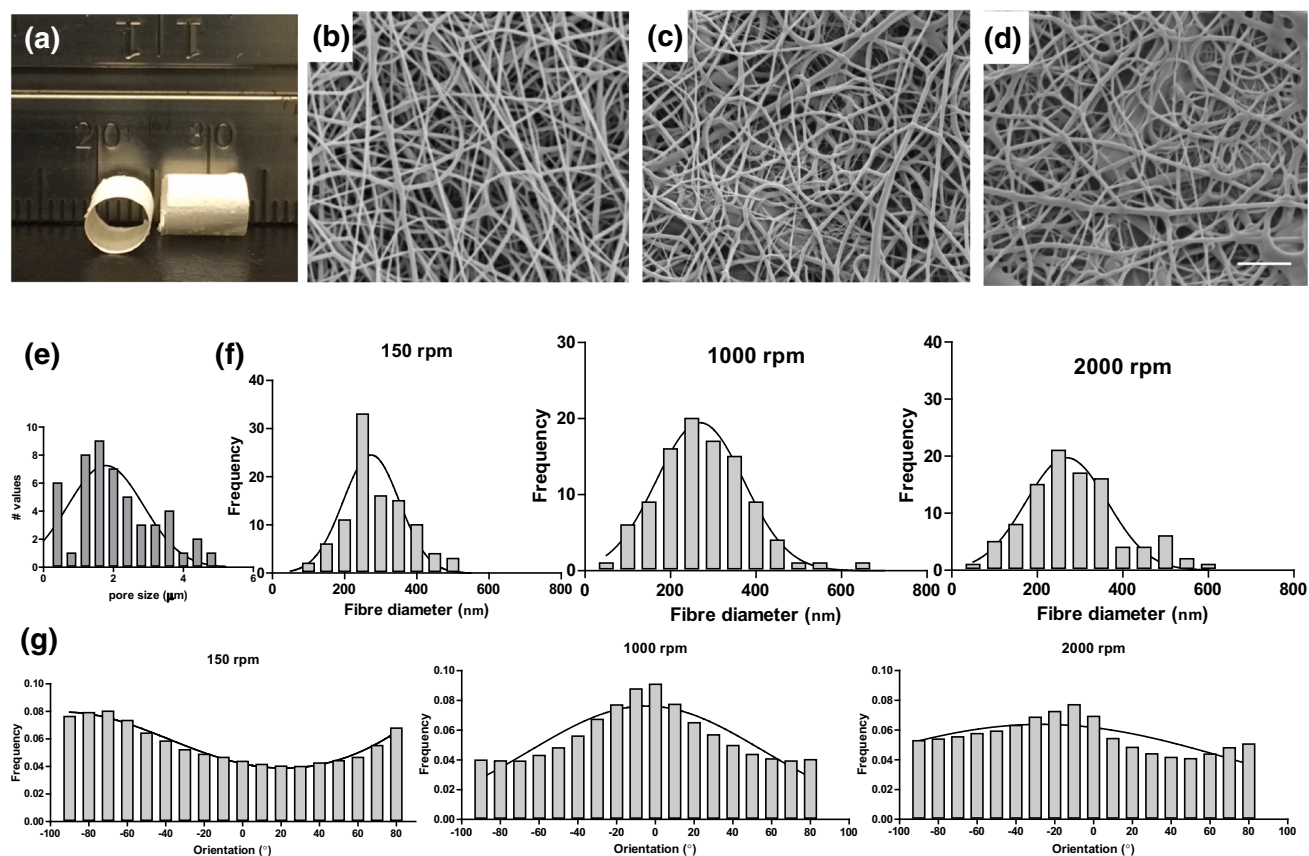


FIGURE 1. Morphological, porosity, fiber diameter and orientation of electrospun tubular PEA vascular scaffolds. (a) Digital image of the tubular scaffolds fabricated with wall thickness of $130\ \mu\text{m}$. (b–d) Representative SEM images of PEA scaffolds fabricated at 150, 1000 and 2000 rpm of the rotating mandrel collector, respectively. (e) Scaffold pore size. The different fiber diameter distributions and respective fiber orientations for the three different rpm are also shown (f, g). Scale bar shown in (d) is $5\ \mu\text{m}$ and is applicable to (b, c).

Although there is an understanding that higher rotational speeds of the mandrel produce smaller fiber diameters, it is often context dependent. For example, in electrospun polyvinylidene fluoride fibers studied by Motamedi *et al.*,²⁵ mean fiber diameter decreased from $520\ \text{nm}$ at $1000\ \text{rpm}$ to $313\ \text{nm}$ at $2000\ \text{rpm}$ before it increased to $463\ \text{nm}$ at $3000\ \text{rpm}$. In another study conducted by Yu *et al.*,⁴⁸ mean fiber diameter decreased from $\sim 750\ \text{nm}$ at $100\ \text{rpm}$ to $\sim 500\ \text{nm}$ at $6000\ \text{rpm}$ for poly (L -lactide-co-glycolide) electrospun fibers. It appears that the role of the collector speed is more impactful at higher fiber diameters than at lower ones. Since our fibers already had a low mean diameter of $\sim 250\ \text{nm}$ at $150\ \text{rpm}$, a further reduction by increasing collector speed up to $2000\ \text{rpm}$ was not possible.²⁴ This is not unexpected as the role of increasing the collector speed is to produce additional stretching of the deposited fibers; however, stretching is finite beyond which it reached the maximal limit.

Similar results were reported for centrifugally spun nanofibres with a spin speed of up to $9000\ \text{rpm}$.⁴⁰

In addition to fiber diameter, the effect of collector rotational speed on the alignment of the fibers was investigated as it was previously shown to have influence fiber orientation and anisotropy.^{17,30,31,48} The preferred orientation of fibers present in the input image (ImageJ software) is the amount in a given direction. It is expected that images that are isotropic to produce a flat histogram instead of a peak at a specific orientation. As shown in Fig. 1g, we did not observe fibers aligned in a specific orientation (0° corresponding to parallel and 90° corresponding to transverse). Instead, the fibers were neither parallel nor transverse which is consistent with the SEM images shown in Fig. 1b–d. For applications such as tendon, cardiac, and neural tissue engineering, electrospun fibers having parallel orientations are considered to be beneficial^{17,31,48} since the microstructures of these tis-

sues are highly aligned in a certain direction and differentiated cells must be guided along with the preferred direction. For the above-mentioned applications, the use of centrifugal forces^{6,40} and controlled electrode geometries^{3,50} and collector speed^{17,30,31,48} were considered as potential tools to impart fiber orientation and anisotropy. Both molecular weight and the polymer concentration of the spinning solution are likely to influence fiber orientation. For instance, PCL fibers spun from a higher concentration and 700–2000 rpm collector speeds were able to form aligned fibers whereas a lower concentration led to random fibers in otherwise same conditions.⁵¹ It is also reported that induction of preferred fiber orientation by collector speed is partly dependent on molecular weight.¹ Since our PEA ($M_w = 55$ kDa, PDI = 2) had a lower molecular weight compared with some commonly used polymers for electrospinning, this may have been a factor for the lack of preferred orientation.

10T1/2 Cell Viability and Proliferation on Electrospun PEA Scaffolds

Having established that the collector speed affected neither the fiber diameter nor the preferred orientation, we tested if these fibrous scaffolds can support mesenchymal multipotent 10T1/2 cell viability, growth, and spreading. Shown in Fig. 2a is cell viability at different culture times. Cells on the fibrous scaffolds were as viable as the positive control tissue culture polystyrene (TCPS) ($p > 0.05$). There was a significant difference between 3 days culture and 7 days culture ($p < 0.05$) and also with 14 days culture ($p < 0.01$ vs. day 3 and $p < 0.05$ vs. day 7) suggesting that cells become increasingly metabolically active. DNA quantification for cultures up to two weeks indicated that cells grew significantly between days three and 14 ($p < 0.01$) (Fig. 2b). In addition to facilitating cell viability and proliferation, PEA fibers must support cell attachment, spreading and infiltration to allow for

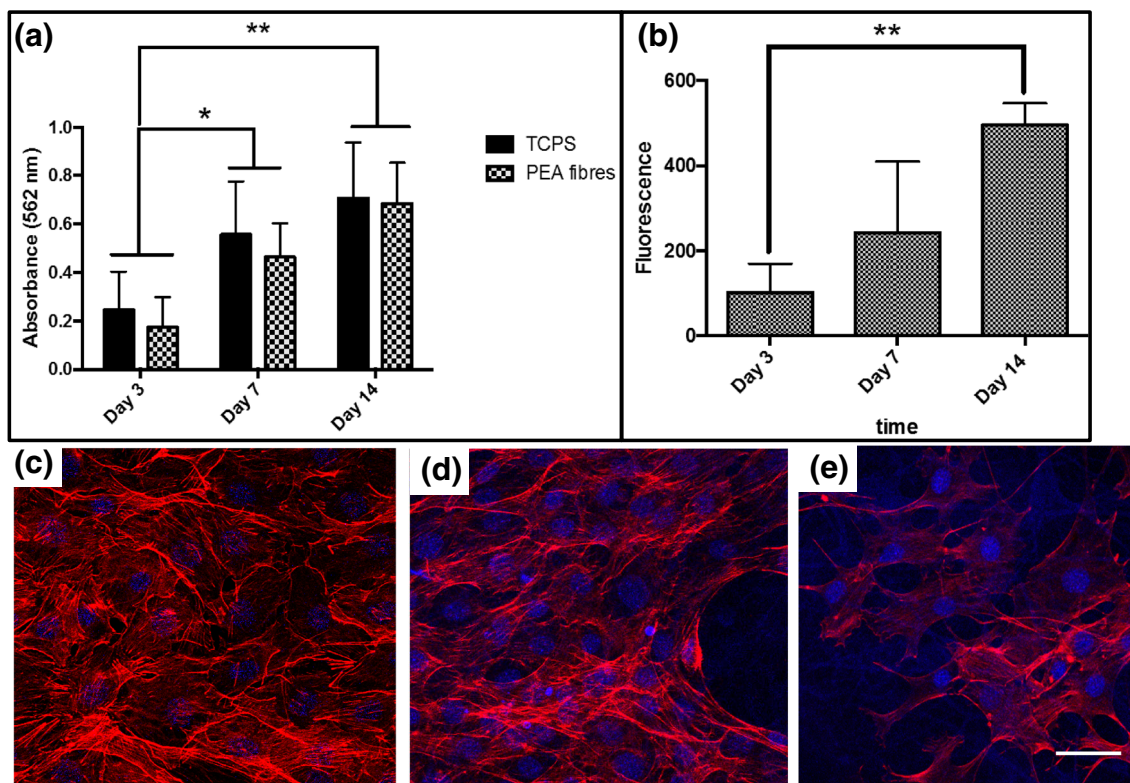


FIGURE 2. 10T1/2 metabolic activity, proliferation, and morphology on PEA fibres. (a) For metabolic activity, scaffolds were seeded with a cell density of 1000 cells/scaffold on 96 well plates and cultured for 3, 7 and 14 days before MTT treatment. Data represents mean \pm SD for three independent experiments conducted in triplicate. Two-way ANOVA and posthoc Tukey comparative tests were used. Solid line coupled with * $p < 0.05$; ** $p < 0.01$. (b) For proliferation 2000 cells/scaffold for the indicated times before performing CyQUANT cell proliferation assay ($n = 6$). One-way ANOVA and posthoc Tukey comparative tests were used. Solid line coupled with ** $p < 0.01$ Absorbance was measured at 480 nm excitation/520 nm emission wavelengths. (c–e) Representative confocal images of 10T1/2 cells cultured on glass coverslips after 3 days of culture (c) and electrospun PEA fibres after 3 days of culture (d) and 7 days of culture (e). Red represents F-actin (phalloidin) and blue represents nuclei (DAPI). Scale bar represents 50 μ m.

cellular in-growth, remodelling and eventual formation of *in vitro* engineered vascular tissues. Given the ability of PEA fibers to support 10T1/2 cell viability and proliferation, 10T1/2 cell-scaffold interactions were assessed using confocal microscopy to understand the influence of the 3D environment on cell attachment, spreading and infiltration over seven days. Morphologically, cells were observed well-spread on the electrospun PEA with abundant F-actin expression and making cell-cell contact (Figs. 2c–2e). Qualitatively, cells on the scaffolds appeared to be well-organized as observed by well-defined F-actin fibers (Fig. 2c).

10T1/2 Cell Infiltration into Electrospun PEA Scaffolds

Compared to other scaffold fabrication techniques such as particulate leaching, gas foaming, and 3D printing that produces large pores, cell infiltration into electrospun scaffolds is challenging because the electrospinning process produces fibers that have smaller pores. If cells can infiltrate readily, the fibrous nature of electrospun scaffolds better mimics the natural extracellular matrix architecture. In the present study, cells started infiltrating the fibrous scaffolds and were observed under the fibers (Fig. 3). Although the pore size of the scaffolds is $\sim 5 \mu\text{m}$ (Fig. 1e), cells were able

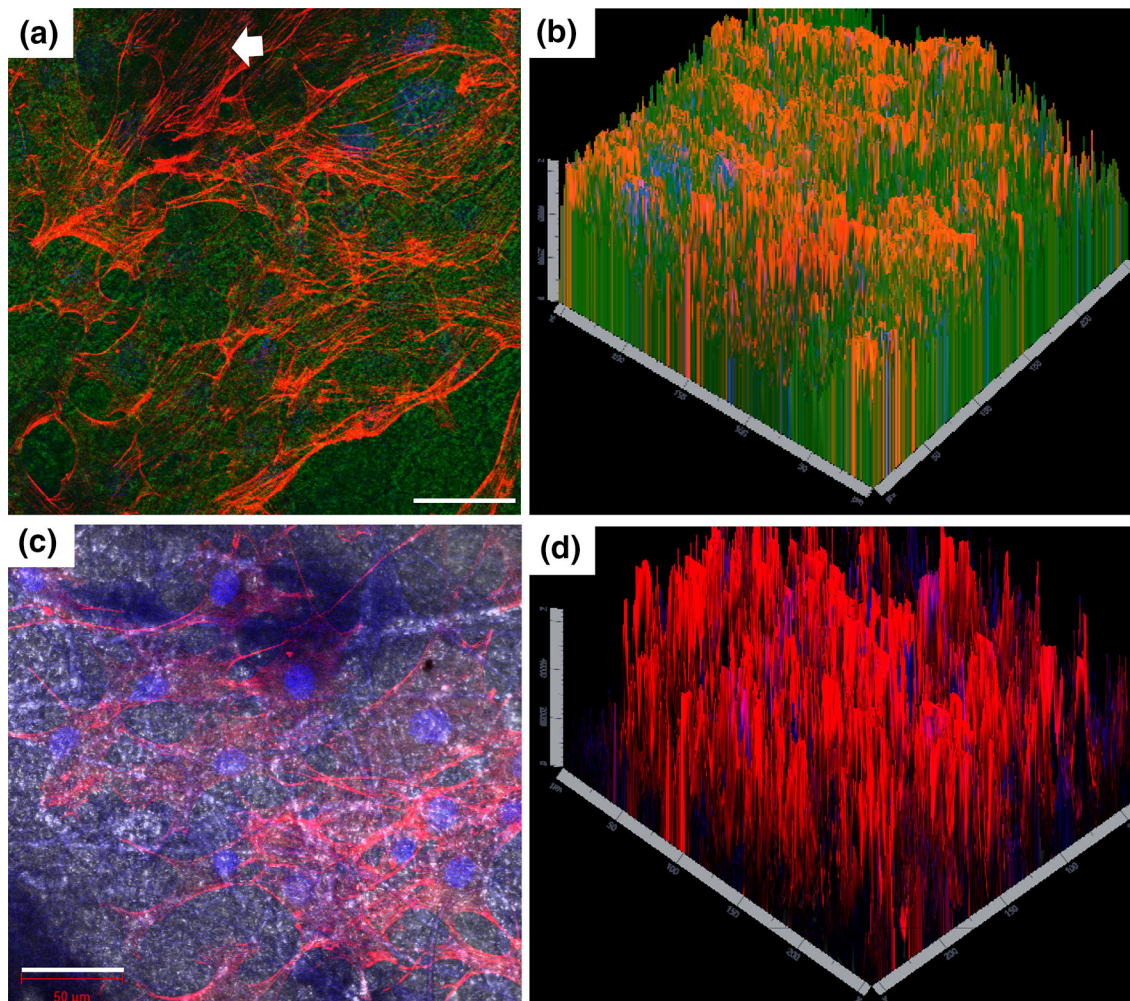


FIGURE 3. Representative confocal microscopy images of mesenchymal progenitor 10T1/2 cells cultured on tubular PEA scaffolds in static conditions for 3 and 7 days. The 2D images (a and c) show cells under the fibers. The 3D reconstruction on a given volume of the scaffolds show cross-section (depth) of infiltration (b and d). Green and grey represent PEA scaffold, red represents F-actin (phalloidin), and blue represents nuclei (DAPI staining). The white arrow in (a) indicates a region where cells are still on the top surface of the PEA. In (d) the PEA fibers signal is omitted from the image for clarity. Scale bar represents $50 \mu\text{m}$.

to wrap within the fiber. In some sections of the scaffolds, cells were still on the top layer (Fig. 3a arrow-head) while the majority have migrated away. The 3D reconstruction of the 2D images for a given volume of the scaffolds showed crosssection (depth) of infiltration by these cells (Figs. 3b and 3d). These results collectively indicated the potential utility of PEA scaffolds to support further cellular activities. In order to increase the pore size that promotes cell infiltration, a number of strategies including the addition of sacrificial microparticles during electrospinning⁴³ and ultrasonication² have been used (more strategies are reviewed in Ref. 45). While more studies are needed to elucidate reasons for the observed data, our studies suggest the possibility that PEAs may provide some physical cues for cell infiltration in the absence of any biochemical gradient.

10T1/2 Cell Differentiation on Electrospun PEA Scaffolds

Given their ability to support 10T1/2 cell attachment, growth, and spreading, and infiltration the possibility of electrospun PEA fibers to support vascular differentiation of progenitor cells was assessed using qPCR and Western blot analyses for smooth muscle alpha-actin (SM- α -actin) and smooth muscle myosin heavy chain (SM-MHC); two important vascular smooth muscle specific markers which represent early and late stage differentiation, respectively. TGF β 1 is a cytokine that has been shown to differentiate 10T1/2 cells to VSMC in 2D cell cultures¹⁵ and to modulate the phenotype of VSMC in 3D culture²³; however, to our knowledge, the *in vitro* vascular differentiation potential of 10T1/2 cells on electrospun 3D scaffolds has not been investigated.

In order to assess the effect of TGF β 1 concentration on VSMC marker gene expression, PEA fibres were affixed to 12-well plates, and seeded with 10T1/2 cells, with TGF β 1 added on day one and qPCR analysis of genes was carried out after 3 days of culture. Data shown in Fig. 4a demonstrated a significant increase in SM- α -actin expression with the addition of 2 ng/mL ($p < 0.05$) and 4 ng/mL TGF β 1 ($p < 0.01$). Late-term differentiation marker SM-MHC expression reached significant levels only with the addition of 4 ng/mL of TGF β 1 ($p < 0.05$). In order to determine if the successful transcription of VSMC markers can lead to translation and subsequent protein expression of early and late markers SM- α -actin and SM-MHC, Western blot analysis was carried out after 7 days of cell culture, with TGF β 1 added on day 1 and day 4 (Fig. 4b). In terms of growth factor addition, TGF β 1 did not have any significant effect on SM- α -actin expression, while SM-MHC protein expression was

upregulated with the addition of 2 ng/mL TGF β 1. Increasing the TGF β 1 concentration to 4 ng/mL did not appear to have an effect on SM-MHC expression; however, this may have been confounded by the potential presence of latent TGF β 1 in serum-based growth media.²⁶ Although the data is limited to draw a comprehensive conclusion from this study, the increase in SM-MHC expression observed suggests that treatment with 2 ng/mL of TGF β 1 was sufficient to induce the differentiation of 10T1/2 cells to vascular smooth muscle on electrospun PEA fibers.

To further confirm 10T1/2 differentiation towards a vascular smooth muscle lineage, immunofluorescent staining was performed on 10T1/2 cells cultured on PEA fibers. As presented in Figs. 4c and 4d, SM- α -actin and SM-MHC were observed in the cross-section demonstrating differentiation on PEA fibers, consistent with the qPCR and Western blot data. Taken together, the results obtained using multiple methodologies as presented in Fig. 4, verified that 10T1/2 cells treated with TGF β 1 on electrospun PEA fibres were able to support 10T1/2 cell differentiation into a vascular smooth muscle lineage, making electrospun PEA scaffolds a potential model to fabricate vascular tissue substitutes for use in preclinical testing. Murine embryonic 10T1/2 cells are multipotent mesenchymal cells with the potential to differentiate into multiple lineages. For instance, 10T1/2 cells have been differentiated to adipogenic,^{16,37} osteogenic,^{22,35} chondrogenic⁴⁹ and endothelial⁴² lineages using a variety of biochemical factors. With regards to smooth muscle differentiation of 10T1/2, there have not been detailed studies. In one study¹⁵ 10T1/2 cells were cocultured with endothelial cells (EC) where EC-induced migration of 10T1/2 cells *via* platelet-derived growth factor-BB was observed. Furthermore, 10T1/2 cells in coculture changed from polygonal to spindle-shaped which was consistent with matured smooth muscle morphology. Treatment of 10T1/2 cells with TGF β induced phenotypic changes in smooth muscle markers similar to those seen in the co-cultures.¹⁵ In all the above-cited studies, no biomaterials were used, and cell cultures were conducted on standard 2D culture systems. Recently, we seeded 10T1/2 cells on porous biostable polyurethane scaffolds and differentiated them to smooth muscle cells.²¹ In the present study, we have extended our previous study²¹ to include biodegradable PEA fibrous scaffolds where 10T1/2 cells have differentiated to smooth muscle cells expressing both SM- α -actin and SM-MHC both at the gene and protein levels.

Given that cells were actively infiltrating the fibrous scaffolds, we investigated the cellular organization at the cross-section. As shown in Fig. 5a, 10T1/2 cells were able to form dense layer cellular bundles. A sec-

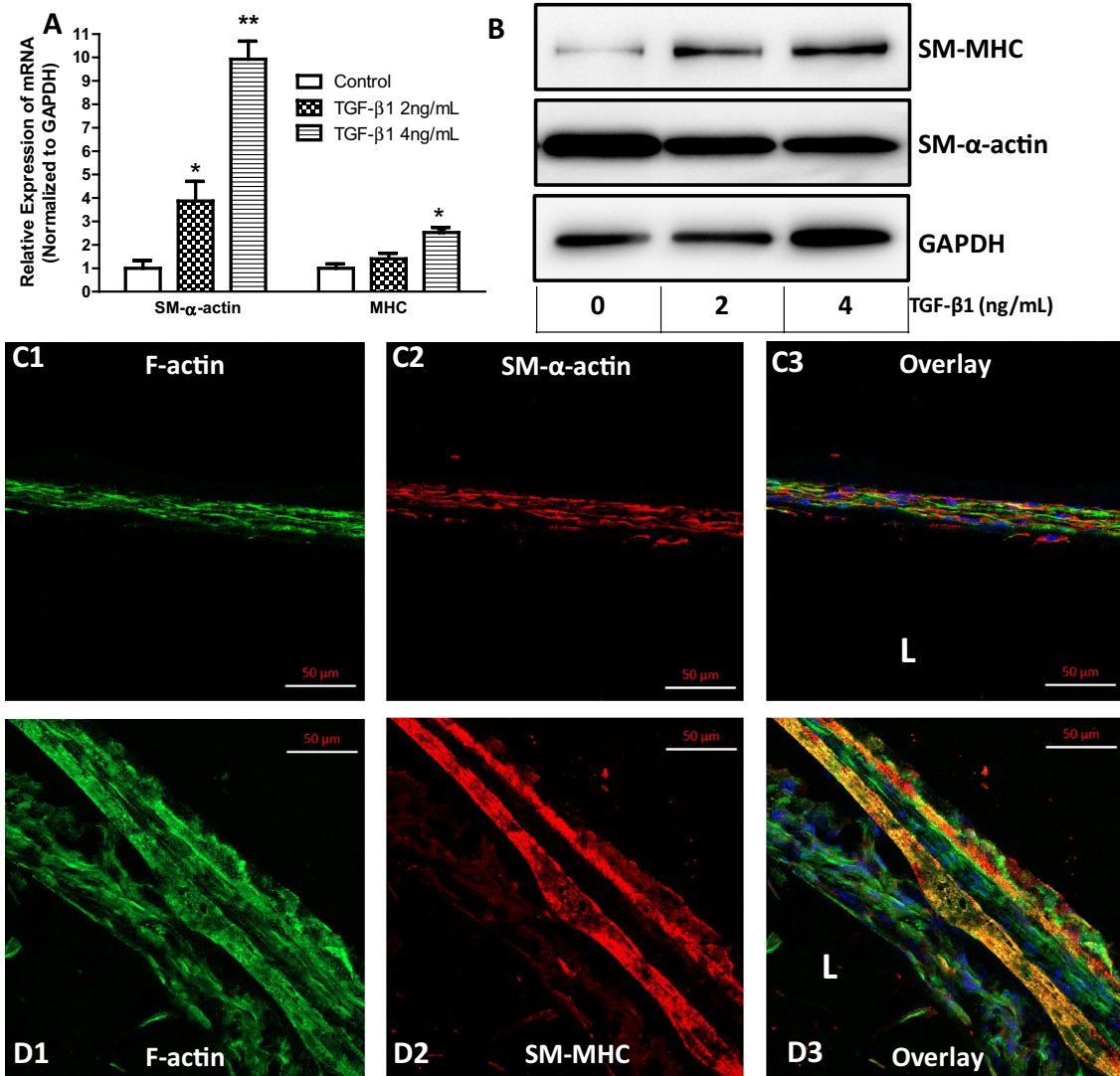


FIGURE 4. Differentiation of 10T1/2 progenitor cells on PEA fibrous scaffolds mediated by TGF- β 1. (a) Quantitative real-time polymerase chain reaction (qPCR) demonstrating 10T1/2 cell expression of smooth muscle α -actin (SM- α -actin) and smooth muscle myosin heavy chain (SM-MHC) genes on PEA fibres treated with 2 ng/mL and 4 ng/mL of TGF- β 1 after 3 days. Results were normalized to GAPDH expression. Statistical significance was analyzed using Student's *t*-test (* $p < 0.05$, ** $p < 0.01$). (b) Western blot analysis demonstrating 10T1/2 expression of SM- α -actin and SM-MHC proteins on PEA fibers after 7 days of culture. 10T1/2 cells were treated with 2 ng/mL and 4 ng/mL of TGF- β 1, respectively. GAPDH was used as a loading control. (c, d) Representative cross-sectional immunostaining and confocal microscopy images of 10T1/2 cells differentiation into smooth muscle cells. Blue in the overlay images is nuclei. Scale bar represents 50 μ m. L stands for lumen side.

tion of the PEA scaffold devoid of cells was visible in areas where cells have not yet infiltrated (arrowhead in Fig. 5b). The tubular scaffolds had $\sim 130 \mu$ m in wall thickness (Fig. 1a), however the scale bars in Fig. 5 indicated that cells have not yet fully infiltrated the entire cross-section. This observation is also consistent with Fig. 3 where cells were seen infiltrating but not to the entire cross-section. In future studies, we will investigate the effect of bioreactor conditions on enhanced cell infiltration and ECM organization.

Since we have previously reported electrospun fibers from a blend of PCL and PEA for elastin expression,³⁴ we also used PCL as a comparator to evaluate if cellular responses on PEAs were consistent with similarly fabricated PCL fibers. Embryonic mesenchymal multipotent cells on both PEA and PCL fibrous scaffolds were similar in cross-sectional view (Figs. 5a and 5c). In terms of elastin expression by differentiated progenitor cells, both elastin and fibrillin-1 were readily and uniformly deposited on both biodegradable fi-

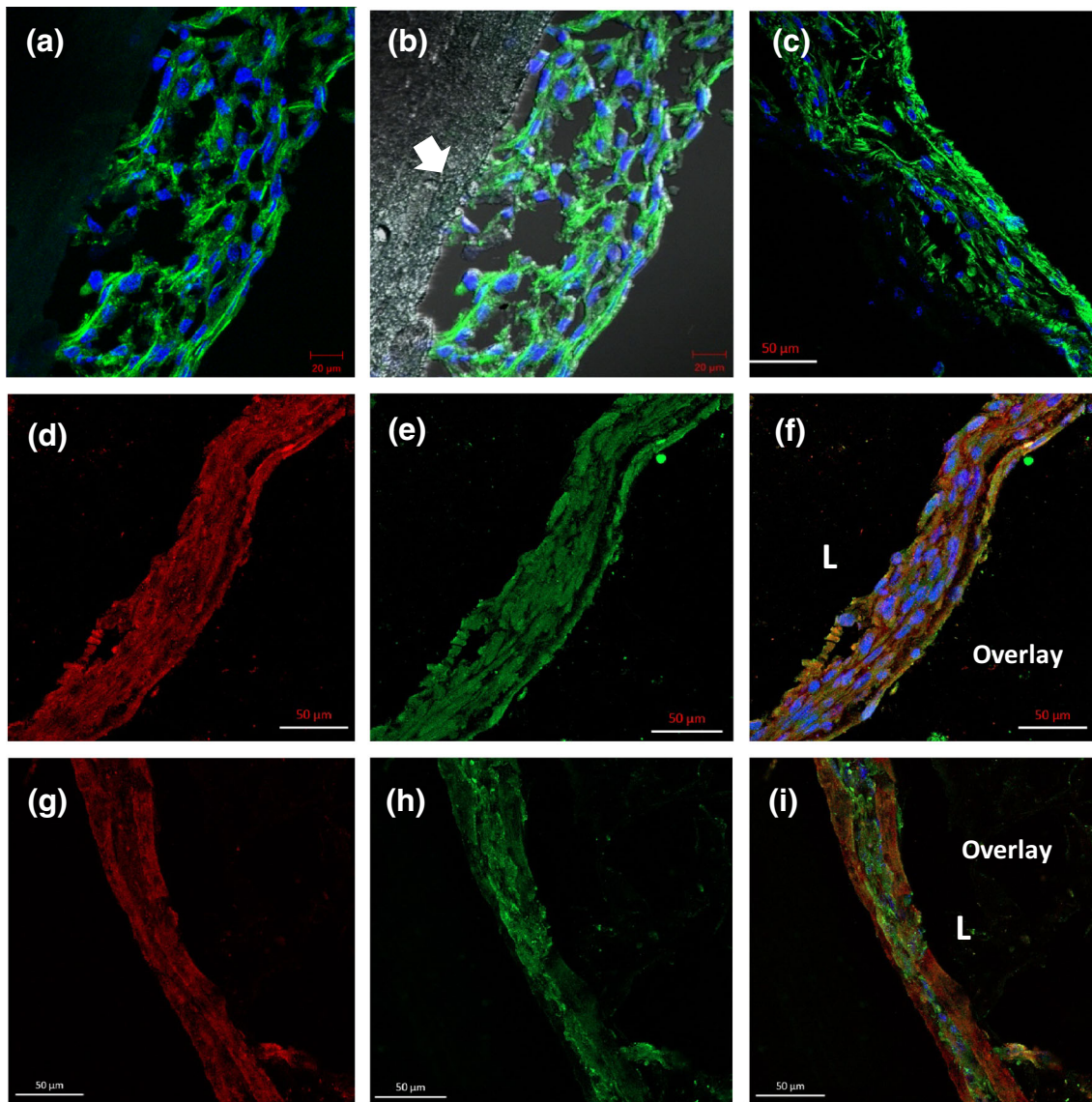


FIGURE 5. Representative cross-sectional confocal microscopy images of 10T1/2 cells expressing elastin and fibrillin. Cells were cultured on tubular fibrous mats and their cross-sectional organization and matrix component expression were analyzed. Green in (a–c) is F-actin whereas in (e, h) it is fibrillin. Red is elastin and blue is nuclei. (c–f) are on PCL fibrous tubular constructs and (a, b, g–i) are for PEA fibrous tubular constructs. Scale bar in (a, b) represents 20 μm whereas C–I it is 50 μm . The arrow in B indicates a section of the scaffold where cells are yet to infiltrate. The scaffold channel is turned off for all other images for clarity. L stands for lumen side.

brous scaffolds (Figs. 5d–5i). Despite many publications on the fabrication of vascular tissues, the absence of substantial elastin in engineered vascular tissue eluded researchers.^{11–13,27} Deposition of the tropoelastin monomer (precursor for elastic fiber) is a necessary but not sufficient condition for fabricating viable engineered vascular tissues. Elastic fiber assembly occurs only in the presence of microfibrils which are primarily composed of fibrillin polymers underscoring its importance for the assembly of elastin into elastic fibers. Fibrillins form microfibrils in elastic tissues and interact with tropoelastin serving as a scaffold

for elastogenesis in elastic tissues such as blood vessels.⁴⁷ We have previously shown that fibrillin-1 was associated with elastin when 10T1/2 cells were differentiated on a porous biostable polyurethane scaffold and produced elastin.²¹ In view elastin's importance in tissue dynamics, our present study on electrospun biodegradable scaffolds confirmed the presence of not only elastin but also fibrillin-1. The scaffolds fabricated in this study had 4 mm internal diameter intended for engineering small diameter vascular tissues (coronary and peripheral arteries). The need for small-diameter vascular substitutes arises because of the difficulty to

replace them by synthetic grafts owing to poor patency. While 10T1/2 cells cannot be used to fabricate clinically-relevant vascular substitutes, they provide a model system to study differentiation and matrix deposition including disease modelling.

Conclusions

The present study explored the utility of biodegradable PEA scaffolds for differentiating murine mesenchymal progenitor cells towards smooth muscle cell lineage. PEA scaffolds were successfully fabricated using electrospinning. Murine mesenchymal progenitor cells differentiated into a smooth muscle cell lineage when seeded on fibrous scaffolds by expressing SM- α -actin and SM-MHC—the latter being a definitive marker for smooth muscle cells. Furthermore, differentiated cells expressed both elastin and fibrillin-1 suggesting the utility of fibrous scaffolds and 10T1/2 cells to fabricate model vascular tissues.

FUNDING

Funding was provided by Natural Sciences and Engineering Research Council of Canada (Grant No. RGPIN-2018-06310).

REFERENCES

- Affi, A. M., H. Yamane, and Y. Kimura. Effect of polymer molecular weight on the electrospinning of polylactides in entangled and aligned fiber forms. *Sen-I Gakkaishi* 66(2):35–42, 2010.
- Aghajanpoor, M., S. Hashemi-Najafabadi, M. Baghaban-Eslaminejad, F. Bagheri, S. Mohammad Mousavi, and F. Azam Sayyahpour. The effect of increasing the pore size of nanofibrous scaffolds on the osteogenic cell culture using a combination of sacrificial agent electrospinning and ultrasonication. *J. Biomed. Mater. Res. A* 105(7):1887–1899, 2017.
- Arras, M. M., C. Grasl, H. Bergmeister, and H. Schima. Electrospinning of aligned fibers with adjustable orientation using auxiliary electrodes. *Sci. Technol. Adv. Mater.* 13(3):035008, 2012.
- Atkins, K. M., D. Lopez, D. K. Knight, K. Mequanint, and E. R. Gillies. A Versatile approach for the syntheses of poly(ester amide)s with Pendant functional groups. *J. Polym. Sci. Part A* 47(15):3757–3772, 2009.
- Awad, N. K., H. Niu, U. Ali, S. Morsi, and T. Lin. Electrospun fibrous scaffolds for small-diameter blood vessels: a review. *Membranes (Basel)* 8(1):15, 2018.
- Badrossamay, M. R., K. Balachandran, A. K. Capulli, H. M. Golecki, A. Agarwal, J. A. Goss, H. Kim, K. Shin, and K. K. Parker. Engineering hybrid polymer-protein super-aligned nanofibers via rotary jet spinning. *Biomaterials* 35(10):3188–3197, 2014.
- Bajpai, V. K., and S. T. Andreadis. Stem cell sources for vascular tissue engineering and regeneration. *Tissue Eng. Part B* 18(5):405–425, 2012.
- Basu, A., K. R. Kunduru, J. Katzhendler, and A. J. Domb. Poly(alpha-hydroxy acid)s and poly(alpha-hydroxy acid-co-alpha-amino acid)s derived from amino acid. *Adv. Drug Deliv. Rev.* 107:82–96, 2016.
- Dahan, N., U. Sarig, T. Bronshtein, L. Baruch, T. Karram, A. Hoffman, and M. Machluf. Dynamic autologous reendothelialization of Small-caliber arterial extracellular matrix: a preclinical large animal study. *Tissue Eng. Part A* 23(1–2):69–79, 2017.
- Dahan, N., G. Zarbiv, U. Sarig, T. Karram, A. Hoffman, and M. Machluf. Porcine small diameter arterial extracellular matrix supports endothelium formation and media remodeling forming a promising vascular engineered bio-graft. *Tissue Eng. Part A* 18(3–4):411–422, 2012.
- Eoh, J. H., N. Shen, J. A. Burke, S. Hinderer, Z. Xia, K. Schenke-Layland, and S. Gerecht. Enhanced elastin synthesis and maturation in human vascular smooth muscle tissue derived from induced-pluripotent stem cells. *Acta Biomater.* 52:49–59, 2017.
- Grenier, S., M. Sandig, D. W. Holdsworth, and K. Mequanint. Interactions of coronary artery smooth muscle cells with 3D porous polyurethane scaffolds. *J. Biomed. Mater. Res. A* 89(2):293–303, 2009.
- Grenier, S., M. Sandig, and K. Mequanint. Smooth muscle alpha-actin and calponin expression and extracellular matrix production of human coronary artery smooth muscle cells in 3D scaffolds. *Tissue Eng. Part A* 15(10):3001–3011, 2009.
- Hao, Y. J., M. Y. Chen, J. B. Zhao, Z. Y. Zhang, and W. T. Yang. Synthesis and properties of polyesteramides having short nylon-610 segments in the main chains through polycondensation and chain extension. *Ind. Eng. Chem. Res.* 52(19):6410–6421, 2013.
- Hirschi, K. K., S. A. Rohovsky, and P. A. D'Amore. PDGF, TGF-beta, and heterotypic cell-cell interactions mediate endothelial cell-induced recruitment of 10T1/2 cells and their differentiation to a smooth muscle fate. *J. Cell Biol.* 141(3):805–814, 1998.
- Huang, H., T. J. Song, X. Li, L. Hu, Q. He, M. Liu, M. D. Lane, and Q. Q. Tang. BMP signaling pathway is required for commitment of C3H10T1/2 pluripotent stem cells to the adipocyte lineage. *Proc. Natl. Acad. Sci. U. S. A.* 106(31):12670–12675, 2009.
- Kim, J. I., T. I. Hwang, L. E. Aguilar, C. H. Park, and C. S. Kim. A controlled design of aligned and random nanofibers for 3D bi-functionalized nerve conduits fabricated via a novel electrospinning set-up. *Sci. Rep.* 6:23761, 2016.
- Knight, D. K., E. R. Gillies, and K. Mequanint. Strategies in functional poly(ester amide) syntheses to study human coronary artery smooth muscle cell interactions. *Biomacromolecules* 12(7):2475–2487, 2011.
- Knight, D. K., E. R. Gillies, and K. Mequanint. Biomimetic L-aspartic acid-derived functional poly(ester amide)s for vascular tissue engineering. *Acta Biomater.* 10(8):3484–3496, 2014.
- Krawiec, J. T., and D. A. Vorp. Adult stem cell-based tissue engineered blood vessels: a review. *Biomaterials* 33(12):3388–3400, 2012.
- Lin, S., and K. Mequanint. Bioreactor-induced mesenchymal progenitor cell differentiation and elastic fiber assem-

- bly in engineered vascular tissues. *Acta Biomater.* 59:200–209, 2017.
- ²²Lin, L., Q. Qiu, N. Zhou, W. Dong, J. Shen, W. Jiang, J. Fang, J. Hao, and Z. Hu. Dickkopf-1 is involved in BMP9-induced osteoblast differentiation of C3H10T1/2 mesenchymal stem cells. *BMB Rep.* 49(3):179–184, 2016.
- ²³Lin, S., M. Sandig, and K. Mequanint. Three-dimensional topography of synthetic scaffolds induces elastin synthesis by human coronary artery smooth muscle cells. *Tissue Eng. Part A* 17(11–12):1561–1571, 2011.
- ²⁴Medeiros, E. S., L. H. C. Mattoso, E. N. Ito, K. S. Gregorski, G. H. Robertson, R. D. Offeman, D. F. Wood, W. J. Orts, and S. H. Imam. Electrospun nanofibers of poly(vinyl alcohol) reinforced with cellulose nanofibrils. *J. Biobased Mater. Bioenergy* 2(3):231–242, 2008.
- ²⁵Motamedi, A. S., H. Mirzadeh, F. Hajjesmaeilbaigi, S. Bagheri-Khoulanjani, and M. Shokrgozar. Effect of electrospinning parameters on morphological properties of PVDF nanofibrous scaffolds. *Prog. Biomater.* 6(3):113–123, 2017.
- ²⁶Oida, T., and H. L. Weiner. Depletion of TGF-beta from fetal bovine serum. *J. Immunol. Methods* 362(1–2):195–198, 2010.
- ²⁷Patel, A., B. Fine, M. Sandig, and K. Mequanint. Elastin biosynthesis: the missing link in tissue-engineered blood vessels. *Cardiovasc. Res.* 71(1):40–49, 2006.
- ²⁸Said, S. S., C. O’Neil, H. Yin, Z. Nong, J. G. Pickering, and K. Mequanint. Concurrent and sustained delivery of FGF2 and FGF9 from electrospun poly(ester amide) fibrous mats for therapeutic angiogenesis. *Tissue Eng. Part A* 22(7–8):584–596, 2016.
- ²⁹Said, S. S., J. G. Pickering, and K. Mequanint. Controlled delivery of fibroblast growth factor-9 from biodegradable poly(ester amide) fibers for building functional neovascu- lature. *Pharm. Res.* 31(12):3335–3347, 2014.
- ³⁰Sensini, A., C. Gualandi, L. Cristofolini, G. Tozzi, M. Dicarolo, G. Teti, M. Mattioli-Belmonte, and M. Letizia Focarete. Biofabrication of bundles of poly(lactic acid)-collagen blends mimicking the fascicles of the human Achilles tendon. *Biofabrication* 9(1):015025, 2017.
- ³¹Sensini, A., C. Gualandi, A. Zucchelli, L. A. Boyle, A. P. Kao, C. Reilly, G. Tozzi, L. Cristofolini, and M. L. Focarete. Tendon fascicle-inspired nanofibrous scaffold of polylactic acid/collagen with enhanced 3D-structure and biomechanical properties. *Sci. Rep.* 8(1):17167, 2018.
- ³²Soffer, L., X. Wang, X. Zhang, J. Kluge, L. Dorfmann, D. L. Kaplan, and G. Leisk. Silk-based electrospun tubular scaffolds for tissue-engineered vascular grafts. *J. Biomater. Sci. Polym. Ed.* 19(5):653–664, 2008.
- ³³Song, H. G., R. T. Rumma, C. K. Ozaki, E. R. Edelman, and C. S. Chen. Vascular tissue engineering: progress, challenges, and clinical promise. *Cell Stem Cell* 22(3):340–354, 2018.
- ³⁴Srinath, D., S. Lin, D. K. Knight, A. S. Rizkalla, and K. Mequanint. Fibrous biodegradable L-alanine-based scaffolds for vascular tissue engineering. *J. Tissue Eng. Regen. Med.* 8(7):578–588, 2014.
- ³⁵Suga, K., M. Saitoh, S. Fukushima, K. Takahashi, H. Nara, S. Yasuda, and K. Miyata. Interleukin-11 induces osteoblast differentiation and acts synergistically with bone morphogenetic protein-2 in C3H10T1/2 cells. *J. Interferon Cytokine Res.* 21(9):695–707, 2001.
- ³⁶Sung, H. J., C. Meredith, C. Johnson, and Z. S. Galis. The effect of scaffold degradation rate on three-dimensional cell growth and angiogenesis. *Biomaterials* 25(26):5735–5742, 2004.
- ³⁷Tang, Q. Q., T. C. Otto, and M. D. Lane. Commitment of C3H10T1/2 pluripotent stem cells to the adipocyte lineage. *Proc. Natl. Acad. Sci. U. S. A.* 101(26):9607–9611, 2004.
- ³⁸Theron, J. P., J. H. Knoetze, R. D. Sanderson, R. Hunter, K. Mequanint, T. Franz, P. Zilla, and D. Bezuidenhout. Modification, crosslinking and reactive electrospinning of a thermoplastic medical polyurethane for vascular graft applications. *Acta Biomater.* 6(7):2434–2447, 2010.
- ³⁹Thottappillil, N., and P. D. Nair. Scaffolds in vascular regeneration: current status. *Vasc. Health Risk Manag.* 11:79–91, 2015.
- ⁴⁰Upson, S. J., T. O’Haire, S. J. Russell, K. Dalgarno, and A. M. Ferreira. Centrifugally spun PHBV micro and nanofibres. *Mater. Sci. Eng C* 76:190–195, 2017.
- ⁴¹Wang, Y., H. Shi, J. Qiao, Y. Tian, M. Wu, W. Zhang, Y. Lin, Z. Niu, and Y. Huang. Electrospun tubular scaffold with circumferentially aligned nanofibers for regulating smooth muscle cell growth. *ACS Appl. Mater. Interfaces.* 6(4):2958–2962, 2014.
- ⁴²Wang, M., Y. Su, H. Sun, T. Wang, G. Yan, X. Ran, F. Wang, T. Cheng, and Z. Zou. Induced endothelial differentiation of cells from a murine embryonic mesenchymal cell line C3H/10T1/2 by angiogenic factors in vitro. *Differentiation* 79(1):21–30, 2010.
- ⁴³Wang, K., M. Zhu, T. Li, W. Zheng, L. Li, M. Xu, Q. Zhao, D. Kong, and L. Wang. Improvement of cell infiltration in electrospun polycaprolactone scaffolds for the construction of vascular grafts. *J. Biomed. Nanotechnol.* 10(8):1588–1598, 2014.
- ⁴⁴Winnacker, M., and B. Rieger. Poly(ester amide)s: recent insights into synthesis, stability and biomedical applications. *Polym. Chem.* 7(46):7039–7046, 2016.
- ⁴⁵Wu, J., and Y. Hong. Enhancing cell infiltration of electrospun fibrous scaffolds in tissue regeneration. *Bioact. Mater.* 1(1):56–64, 2016.
- ⁴⁶Xie, C., R. P. Ritchie, H. Huang, J. Zhang, and Y. E. Chen. Smooth muscle cell differentiation in vitro: models and underlying molecular mechanisms. *Arterioscler. Thromb. Vasc. Biol.* 31(7):1485–1494, 2011.
- ⁴⁷Yanagisawa, H., and E. C. Davis. Unraveling the mechanism of elastic fiber assembly: the roles of short fibulins. *Int. J. Biochem. Cell Biol.* 42(7):1084–1093, 2010.
- ⁴⁸Yu, J., A. R. Lee, W. H. Lin, C. W. Lin, Y. K. Wu, and W. B. Tsai. Electrospun PLGA fibers incorporated with functionalized biomolecules for cardiac tissue engineering. *Tissue Eng. Part A* 20(13–14):1896–1907, 2014.
- ⁴⁹Zhao, L., G. Li, K. M. Chan, Y. Wang, and P. F. Tang. Comparison of multipotent differentiation potentials of murine primary bone marrow stromal cells and mesenchymal stem cell line C3H10T1/2. *Calcif. Tissue Int.* 84(1):56–64, 2009.
- ⁵⁰Zhao, J. H., H. Y. Liu, and L. Xu. Preparation and formation mechanism of highly aligned electrospun nanofibers using a modified parallel electrode method. *Mater. Des.* 90:1–6, 2016.
- ⁵¹Zhu, Y., Y. Cao, J. Pan, and Y. Liu. Macro-alignment of electrospun fibers for vascular tissue engineering. *J. Biomed. Mater. Res. B* 92(2):508–516, 2010.

Publisher’s Note Springer Nature remains neutral with regard to jurisdictional claims in published maps and institutional affiliations.